

# BRCA2 Fine-Tunes the Spindle Assembly Checkpoint through Reinforcement of BubR1 Acetylation

Eunhee Choi,<sup>1,6</sup> Pil-Gu Park,<sup>1,6</sup> Hae-ock Lee,<sup>1,6,7</sup> Yoo-Kyung Lee,<sup>1</sup> Gyeong Hoon Kang,<sup>2</sup> Jong Won Lee,<sup>3,4</sup> Wonshik Han,<sup>3</sup> Ho Chang Lee,<sup>2</sup> Dong-Young Noh,<sup>3</sup> Sergey Lekomtsev,<sup>5</sup> and Hyunsook Lee<sup>1,\*</sup>

<sup>1</sup>Department of Biological Sciences and Institute of Molecular Biology and Genetics, Seoul National University, 599 Gwanak-Ro, Gwanak-ku, Seoul 151-742, Korea

<sup>2</sup>Department of Pathology

<sup>3</sup>Department of Surgery and Cancer Research Institute

Seoul National University, College of Medicine, Seoul 110-744, Korea

<sup>4</sup>Department of Surgery, Asan Medical Center, University of Ulsan College of Medicine, Seoul 138-736, Korea

<sup>5</sup>Cancer Research UK London Research Institute, Clare Hall Laboratories, Blanche Lane, South Mimms, Hertfordshire EN6 3LD, UK

<sup>6</sup>These authors contributed equally to this work

<sup>7</sup>Present address: Department of Pathology, Korea University School of Medicine, Seoul 135-710, Korea

\*Correspondence: HL212@snu.ac.kr

DOI 10.1016/j.devcel.2012.01.009

## SUMMARY

Germline mutations that inactivate *BRCA2* promote early-onset cancer with chromosome instability. Here, we report that *BRCA2* regulates the spindle assembly checkpoint (SAC). Previously, we reported that BubR1 acetylation is essential for SAC activity. In this study we show that *BRCA2* recruits the PCAF acetyltransferase and aids in BubR1 acetylation during mitosis. In the absence of *BRCA2*, BubR1 acetylation is abolished, and the level of BubR1 decreases during mitosis. Similarly, *Brca2*-deficient mouse embryonic fibroblasts exhibited weak SAC activity. Transgenic mice that were engineered to have interruptions in the *BRCA2*-BubR1 association exhibited marked decrease of BubR1 acetylation, weakened SAC activity, and aneuploidy. These transgenic mice developed spontaneous tumors at 40% penetrance. Moreover, immunohistochemical analyses of human breast cancer specimens suggested that *BRCA2* mutation and BubR1 status is closely linked. Our results provide an explanation for how mutation of *BRCA2* can lead to chromosome instability without apparent mutations in SAC components.

## INTRODUCTION

*BRCA2*-deficient tumors exhibit chromosome instability, manifested by aneuploidy with chromosome translocations (Lee et al., 1999; Venkitaraman, 2002). Spontaneous translocation and radially structured chromosomes arise due to a loss of regulating Rad51 during homologous recombination (HR) and repair (Pellegrini and Venkitaraman, 2004; Venkitaraman, 2002; West, 2003), consistent with the finding that *BRCA2* is also *FANCD1*, the gene mutated in the Fanconi anemia (Hirsch et al., 2004; Howlett et al., 2002).

Compared to the involvement of *BRCA2* in HR and the basis of chromosome structure instability, the molecular mechanisms underlying the chromosome number instability of *BRCA2*-deficient cells are not as well understood. A number of studies report a direct role of *BRCA2* at the cytokinetic midbody (Daniels et al., 2004; Lee et al., 2011), suggesting that the tumor-suppressive function of *BRCA2* is not restricted to regulation of DNA repair but involves correct cell division. Failure of cytokinesis (completion of cell division) results in binucleated cells and polyploidy, as has been observed in the *Brca2*-inactivated mouse model (Rowley et al., 2011). Although cytokinetic failure can eventually contribute to aneuploidy, unequal segregation of duplicated chromosomes is the major cause of aneuploidy, particularly the early-onset aneuploidy. Therefore, we hypothesized that disruption of *BRCA2* may directly interfere with proper chromosome segregation and contribute to aneuploidy.

Mitotic fidelity, the accurate segregation of chromosomes, is guaranteed by the spindle assembly checkpoint (SAC). The SAC ensures that each daughter cell receives the full complement of chromosomes after cell division by checking that all chromosomes are attached to spindles in a bipolar manner (Yu, 2002). From the unattached kinetochore a diffusible “wait anaphase” signal is generated and amplified (Kulukian et al., 2009). Ultimately, the SAC inhibits APC/C E3 ligase activity, and the proteolysis of cyclin B is delayed. When the checkpoint fails, cells either die or become aneuploid (Rieder and Maiato, 2004). In prometaphase, BubR1 recycles rapidly between kinetochore and cytosol, binds to both APC/C and its coactivator Cdc20, is a potent inhibitor of APC/C (Peters, 2006), monitors chromosome spindle attachments (Ditchfield et al., 2003; Lampson and Kapoor, 2005), and regulates mitotic timing (Choi et al., 2009; Meraldi et al., 2004). Previously, we reported that BubR1 is acetylated by PCAF acetyltransferase at prometaphase and that the acetylated BubR1 inhibits APC/C. When checkpoint is satisfied, BubR1 is deacetylated and becomes a substrate of APC/C-Cdc20 (Choi et al., 2009; Yekezare and Pines, 2009).

In yeast two-hybrid screens, *BRCA2* was found to bind to BubR1 (Futamura et al., 2000). However, the physiological outcome of the *BRCA2*-BubR1 interaction remains unclear.

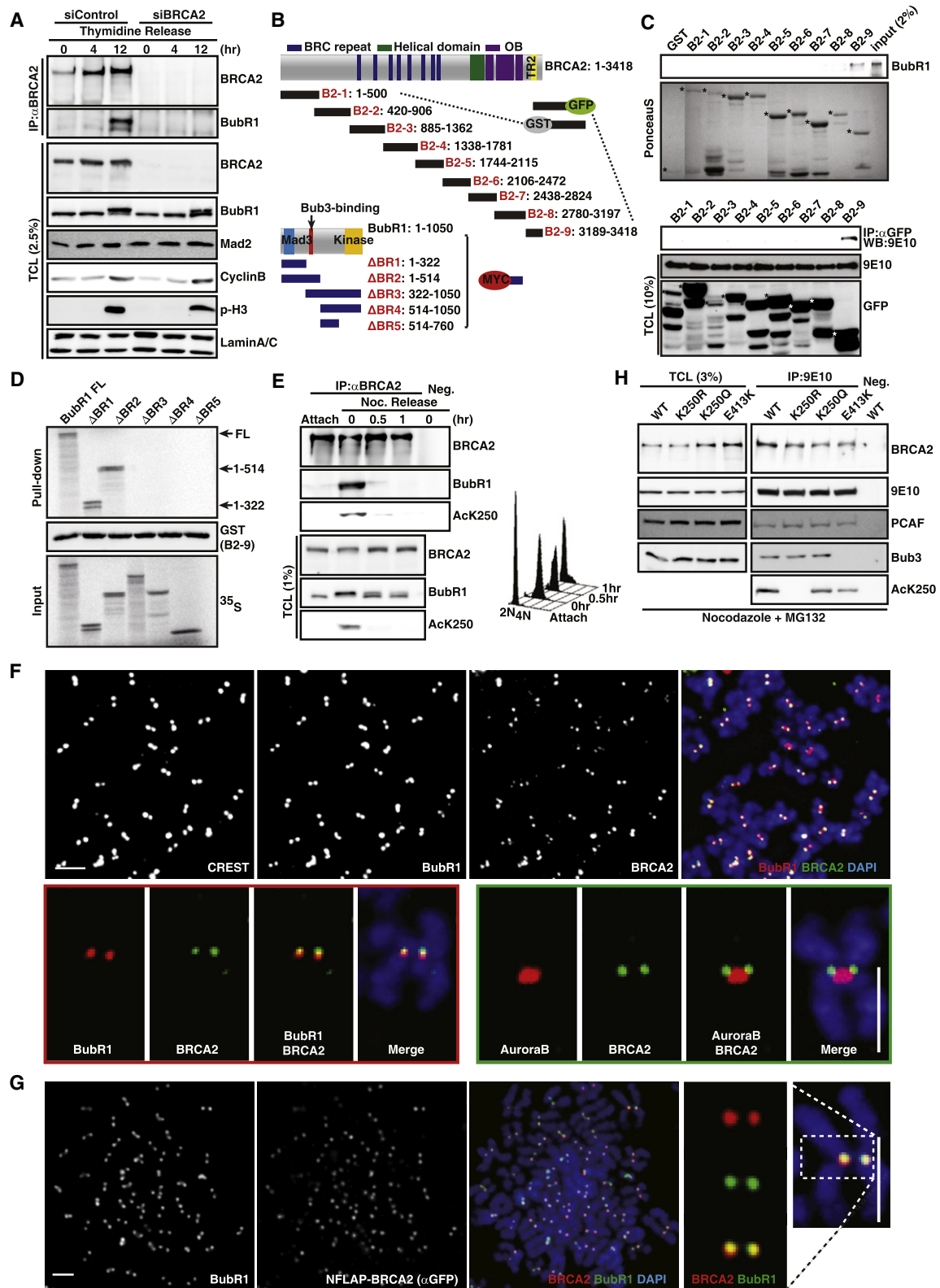


**Figure 1. BRCA2 Forms a Complex with BubR1 in Prometaphase**

(A) HeLa cells transfected with indicated siRNAs were synchronized by double-thymidine block and released. Cells were harvested at the indicated time points after release and subjected to IP with a BRCA2 antibody (sh-hB2-4, Figure S1E) and WB with BubR1 and BRCA2 antibodies (Calbiochem, Ab-1). TCLs (2.5%) were subjected to WB with the indicated antibodies. WB with anti-Mad2 was included to control for off-target effects of siRNA.

Interestingly, *in vitro* studies have suggested that the N terminus of BRCA2 binds to PCAF (Fuks et al., 1998). Together, we hypothesized that BRCA2 may be involved in the process of BubR1 acetylation in mitosis by serving as a scaffold for interaction between PCAF and BubR1. Here, we show that BRCA2 recruits PCAF and mediates the association and acetylation of BubR1; BRCA2 is involved in proper control of mitosis. This study reveals the role of BRCA2 in chromosome segregation and provides an explanation for aneuploidy in *BRCA2*-deficient cells.

## RESULTS

### BRCA2 Associates with BubR1 in Prometaphase

To elucidate the mitotic role of BRCA2, we first confirmed the physical association between BRCA2 and BubR1. The results indicated that BRCA2 and BubR1 form a complex during mitosis, 12 hr after thymidine release, as shown by the levels of cyclin B and phospho-histone H3 (pH3) (Figure 1A).

We generated a series of deletion mutants to map the interaction domains (Figure 1B) and found that the N terminus (amino acids 1–514) of BubR1, the region essential for its checkpoint activity (Malureanu et al., 2009), physically interacts with the extreme C terminus of BRCA2 (amino acids 3,189–3,418; Figures 1B–1D; see Figure S1 available online). This region of BRCA2 is involved in the stability of oligomerized Rad51 filaments (Davies and Pellegrini, 2007) and contains CDK1 phosphorylation sites (Esashi et al., 2007).

Next, we determined the timing of BRCA2/BubR1 complex formation during mitosis. HeLa cells were synchronized at prometaphase by nocodazole (Noc) treatment, released into the mitotic cell cycle, and subjected to immunoprecipitation (IP) and western blotting (WB). Importantly, BubR1 was detected only in BRCA2 immune complex of Noc-arrested cells (Figure 1E), indicating that BRCA2/BubR1 complex forms predominantly during prometaphase. Notably, BRCA2-bound BubR1 was acetylated, as detected by WB results using an AcK250 antibody (Figure 1E,  $\alpha$ AcK250) (Choi et al., 2009).

BubR1 localizes to kinetochores, where it ensures bipolar spindle attachments and is involved in checkpoint signaling

(Elowe et al., 2007; Logarinho and Bousbaa, 2008). Therefore, we first assessed whether the BRCA2-BubR1 complex was present at the prometaphase kinetochore. In chromosome spreads coupled with immunofluorescence, we observed that BRCA2 was associated with BubR1 at the outer kinetochores (Figure 1F, red box). By contrast, Aurora B, which localizes to the inner centromeres (Vagnarelli and Earnshaw, 2004), did not overlap with BRCA2 (Figure 1F, green box).

To exclude the possibility that the BRCA2 antibody detected the kinetochore nonspecifically, BRCA2 localization was examined in HeLa cells expressing full-length bacterial artificial chromosome (BAC)-encoded N terminus FLAP-tagged BRCA2 (NFLAP-BRCA2) (Lekomtsev et al., 2010). The result showed that approximately 47% of green fluorescent protein (GFP) fluorescence overlapped with CREST immunofluorescence (Figure S1D). In chromosome spreads coupled with immunofluorescence, BRCA2 colocalization with BubR1 was confirmed (Figure 1G).

BRCA2 binding to BubR1 was not restricted to the kinetochores because the cytosolic BubR1 mutant E413K that retains the ability to inhibit APC/C-Cdc20 (Malureanu et al., 2009) could bind to BRCA2 (Figures 1H and S1C). E413K was also acetylated in prometaphase (Figure 1H, AcK250). Collectively, these data led us to hypothesize that BRCA2 participates in a regulatory pathway involving BubR1 acetylation and SAC activity.

### BRCA2 Is Required for BubR1 Acetylation

The failure of BubR1 acetylation results in premature degradation of BubR1 in prometaphase and shortened mitotic timing (Choi et al., 2009). To address whether BRCA2 is involved in BubR1 acetylation, we analyzed mitotic BubR1 levels in HeLa cells transfected with siRNAs against *BRCA2*. The results indicate that the level of BubR1, but not that of Bub1, was markedly decreased at prometaphase kinetochores, when BRCA2 was depleted (Figure 2A). The decrease in BubR1 levels at kinetochores fits with the elevated levels of ubiquitination and subsequent degradation of BubR1 when BRCA2 is depleted (Figure 2B). Consistently, BubR1 acetylation at K250 was markedly reduced after silencing *BRCA2* (Figure 2B, AcK250), which was restored upon expression of *FLAG-BRCA2* (Figure S2A).

(B) Schematic illustration of the various BRCA2-deletion (upper panel; see also Figure S1A) and BubR1-deletion constructs (lower panel). The functional motifs reported are marked. BRCA2 deletion constructs were tagged with GFP or GST, and BubR1 deletion constructs were myc tagged at the N terminus.

(C) A series of GST-fused BRCA2 deletion mutants were purified from *E. coli*. One microgram of each recombinant BRCA2 GST-fusion protein bound to Sepharose 4B beads was incubated with *in vitro*-translated and  $^{35}$ S-labeled BubR1 (Myc tagged) and analyzed. A Ponceau S-stained blot is included to normalize the recombinant proteins in the reaction (upper panel). The mapping of the BubR1-interacting BRCA2 domain was confirmed by transfection in 293T cells followed by IP (anti-GFP) and WB analyses (9E10). The same blot was reprobed with anti-GFP (lower panel).

(D) Two micrograms of GST-B2-9 (BubR1-interacting BRCA2 C terminus) were incubated with a series of  $^{35}$ S-labeled BubR1 deletion mutants and analyzed.

(E) BRCA2 and BubR1 interact in mitosis. HeLa cells were synchronized with Noc and mitotic shake off, and then were released. The cell-cycle profile was assessed by flow cytometry (right). At the indicated times, cells were harvested and subjected to IP with anti-BRCA2 (sh-hB2-4) and WB with anti-BubR1, anti-BRCA2 (Ab-1) and anti-AcK250. Lysates from attached cells (Attach) served as an interphase control. Neg, negative control.

(F) BRCA2 colocalizes with BubR1 at prometaphase kinetochores. Metaphase chromosome spreads from HeLa cells were coimmunostained with CREST, anti-BRCA2 (Calbiochem, Ab-2), and anti-BubR1 or anti-Aurora B. Photographs were taken at 1,000 $\times$  magnification under a DeltaVision RT microscope. Enlarged images of single chromosomes in each setting are shown (lower panel). Scale bar, 5  $\mu$ m.

(G) Kinetochore localization of BRCA2 was confirmed in HeLa cells expressing BAC-encoded GFP-BRCA2. BRCA2 was detected with anti-GFP. Enlarged images of single chromosomes are shown (right panel). Scale bar, 5  $\mu$ m.

(H) Cytosolic BubR1 mutant also interacts with BRCA2 and is acetylated. 293T cells were cotransfected with Myc-tagged BubR1 mutants (*Myc-BubR1 WT*, *-K250R*, *-K250Q*, *-E413K*) and *BRCA2* encoding plasmids. K250Q is the acetylation-mimetic form and K250R is the acetylation-deficient form of BubR1 (Choi et al., 2009). Cells kept in mitosis with Noc and MG132 treatment were subjected to IP with 9E10 and WB with anti-BRCA2 (Ab-1), -PCAF, -Bub3, and -AcK250. Neg, negative control. See also Figure S1.

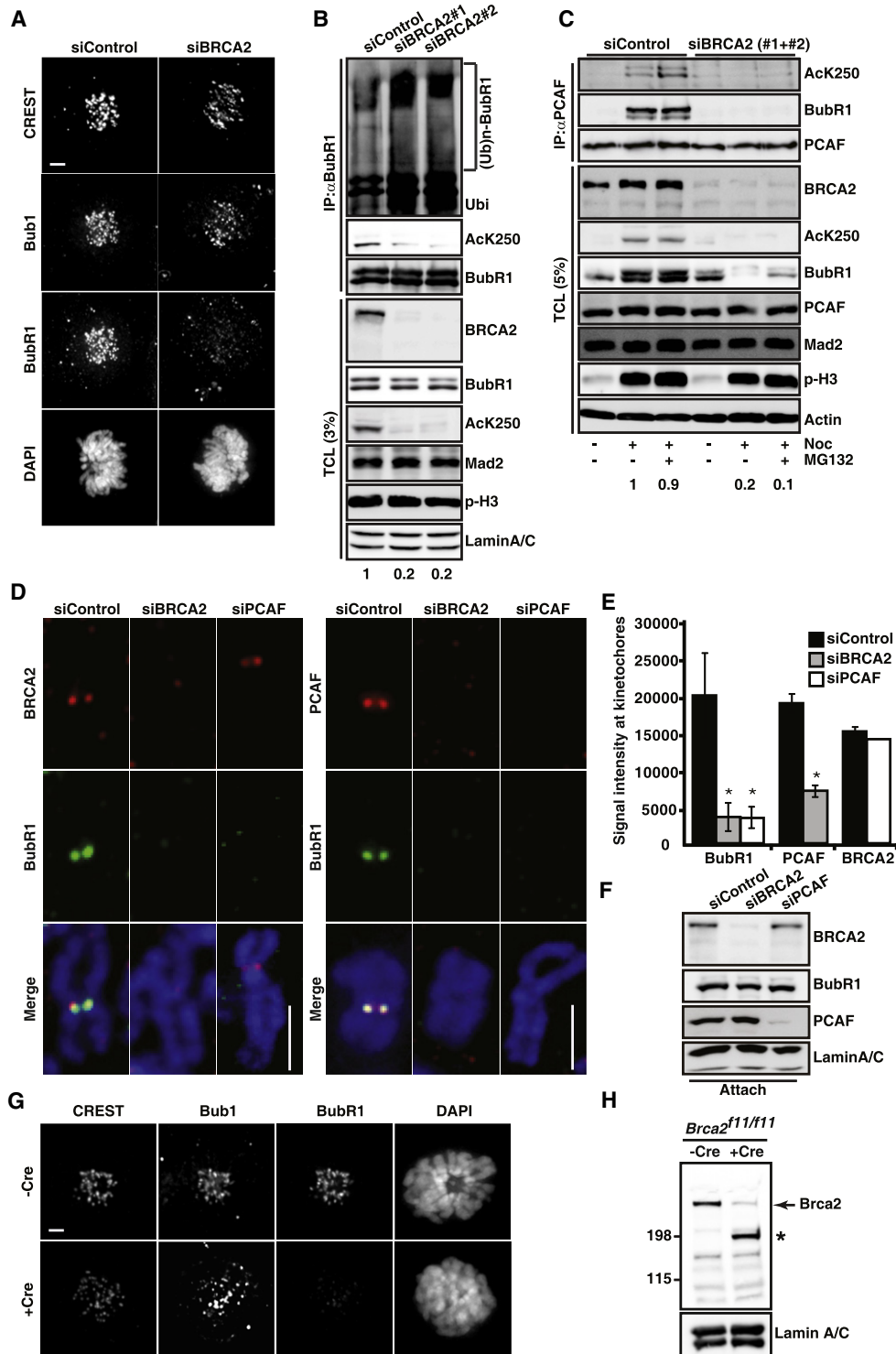


**Figure 2. BRCA2 Is Required for PCAF-Mediated BubR1 Acetylation**

(A) HeLa cells transfected with indicated siRNAs were subjected to coimmunostaining with CREST and anti-BubR1 or anti-Bub1. Prometaphase cells are presented. Scale bar, 5  $\mu$ m.

(B) HeLa cells transfected with two different siRNAs against *BRCA2* were Noc arrested and treated with MG132 then subjected to IP with a BubR1 antibody and WB with the indicated antibodies (in B, C, and F, anti-BRCA2 [Calbiochem, Ab-1] was used). The intensities of BubR1 and AcK250 were measured using the densitometer (Multi Gauge), and the ratio of AcK250/total BubR1 in each lane, relative to siControl, is marked.

(C) HeLa cells transfected with indicated siRNAs were treated with the drugs indicated. The levels of each protein in anti-PCAF immunoprecipitates and TCL were analyzed by WB. Numbers at the bottom indicate the ratio of AcK250/total BubR1 in each lane, relative to the siControl.

These data suggest that BRCA2 contributes to regulation of BubR1 acetylation.

Next, we asked how BRCA2 participates in BubR1 acetylation. BRCA2 does not possess innate acetyltransferase activity (Figure S2B). Therefore, we tested whether BRCA2 affected the association between PCAF and BubR1. We examined PCAF immune complexes in HeLa cells transfected with siRNAs against *BRCA2* and compared them with those of the control. In control cells PCAF and BubR1 binding, and BubR1 acetylation, was detected exclusively in mitosis, i.e., in Noc-arrested cells and in cells treated with Noc followed by MG132 (Figure 2C, siControl). In comparison, BubR1 disappeared from PCAF immune complexes when cells were depleted of BRCA2 (Figure 2C, siBRCA2). Consistently, BubR1 acetylation was detected in total cell lysates (TCLs) of control mitotic cells, but not in cells depleted of BRCA2 (Figure 2C,  $\alpha$ AcK250). IP with an AcK250 antibody and WB with a PCAF or BubR1 antibody gave consistent results (Figure S2C), suggesting that BRCA2 is required and may serve as a scaffold for the binding of BubR1 and PCAF during prometaphase.

To confirm that BRCA2 serves as a platform for PCAF-BubR1 binding, we measured the protein levels at the kinetochore (Figures 2D–2F). Knockdown of *BRCA2* by siRNA resulted in a 4-fold reduction in BubR1 and PCAF levels (Figures 2D, 2E, S2D, and S2E, siBRCA2). Depletion of PCAF resulted in a similar level of BubR1 reduction (Figures 2D, 2E, S2D, and S2E, siPCAF); however, the BRCA2 level was unchanged when PCAF was depleted (Figures 2D and 2E, siPCAF). The reduction in BubR1 levels after depletion of BRCA2 or PCAF was restored when cells were treated with MG132 at the kinetochore and in whole cell (Figures S2F and S2G), indicating that the reduction resulted from proteolysis, and not the failure in localization at the kinetochore.

The requirement of BRCA2 in BubR1 acetylation and maintenance in prometaphase was confirmed in mouse embryonic fibroblasts (MEFs) isolated from *Brca2* (mouse *BRCA2*)-conditional knockout mice. When the *Brca2* allele was disrupted in *Brca2*<sup>f1/f1</sup> MEFs (Jonkers et al., 2001) after infection with an adenovirus expressing Cre recombinase (Ad-Cre), the levels of BubR1 markedly decreased in prometaphase, whereas Bub1 was unchanged (Figure 2G). In *Brca2*<sup>f1/f1</sup> MEFs, exon 11 is deleted, but others are expressed in frame (Figure 2H) (Jonkers et al., 2001). Therefore, this result suggests that in addition to the BubR1-binding C terminus (Figures 1 and S1) and the N-terminal PCAF-binding domains (Fuks et al., 1998), the domain encoded by exon 11 of *Brca2* is required for BubR1 to be properly acetylated and maintain adequate levels at the prometaphase kinetochore.

### BRCA2 Controls SAC Activity by Regulating BubR1 Acetylation

Next, we examined the contribution of BRCA2 in SAC activity. First, we assessed the response to microtubule poisoning by measuring the mitotic index; that is the proportion of cells arrested in mitosis upon Noc treatment. The mitotic index was determined by measuring the number of 4C cells that finished replication and were positive for mitotic protein monoclonal 2 (MPM2) immunostaining, which specifically detects phosphoproteins in mitosis (Davis et al., 1983). Twenty-four hours post-Noc treatment, approximately 68% of HeLa cells exhibited MPM2 positivity, indicating that the SAC was intact (Choi et al., 2009; Davis et al., 1983) (Figure 3A, siControl, blue diamonds). In contrast, BubR1-depleted cells lost the typical MPM2 peak following Noc treatment, indicating that their SAC was compromised (Figure 3A, siBubR1, green triangles). Cells transfected with siRNAs against *BRCA2* exhibited markedly less MPM2 staining compared with control cells, indicating weakened SAC activity (Figure 3A, siBRCA2, red rectangles).

Because BRCA2 plays crucial roles in double-stranded DNA break repair, depleting BRCA2 results in DNA damage that might interfere with entry into mitosis. We checked the cell-cycle profiles at the time of SAC analysis. The result showed that depleting BRCA2 did not change the cell-cycle profile in our experimental setting (Figure S3C). Analysis of  $\gamma$ -H2AX staining (Figures S3D and S3E) and metaphase chromosomes (Figure S3H, lower panel) also indicated that DNA damage was not significant at 48 hr post-*BRCA2* depletion. These results suggest that the weakened SAC activity in *BRCA2*-depleted cells is not the secondary effect from impaired mitotic entry.

To confirm the result, we assessed the SAC activity by counting the number of 5' bromodeoxyuridine (BrdU)-positive mitotic cells (pH3 positive) after BrdU pulse and Noc treatment (Jeong et al., 2010) (Figures 3B and S3A). Up to 80% of mitotic cells were BrdU-positive at 15.5 hr post-Noc treatment, which decreased at 21.5 hr, a pattern similar to MPM2 staining. In comparison, cells depleted of BubR1 or BRCA2 displayed dramatic decrease of BrdU-positive mitotic cells. This result confirms that the absence of BRCA2 weakens SAC activity (Figures 3B, S3A, and S3B).

In an accompanying experiment, micronuclei were frequently observed in BubR1- and BRCA2-depleted cells, which increased with time after Noc treatment (Figure 3C). These data suggest that, similar to BubR1-depleted cells, BRCA2-depleted cells display failures in accurate chromosome segregation and mitotic infidelity.

Next, we assessed the mitotic timing in MEFs derived from *Brca2* conditional knockout mice (Jonkers et al., 2001). MEFs

(D) HeLa cells transfected with indicated siRNAs were treated with 100 ng/ml Noc for 6 hr, subjected to mitotic shake off, and the metaphase chromosome spreads were prepared, followed by immunostaining with anti-BRCA2 (Calbiochem, Ab-2), anti-BubR1, and anti-PCAF antibodies. Scale bar, 5  $\mu$ m.

(E) Fluorescence intensity at kinetochores (D) was measured using ImageJ and depicted as histograms. The results are from two independent experiments (mean  $\pm$  SEM;  $n \geq 5$  prometaphase cells: siControl [ $n = 1,524$  kinetochores]; siBRCA2 [ $n = 1,089$ ]; siPCAF [ $n = 294$ ]). Asterisks mark significant differences from the siControl calculated by a t test ( $p < 0.0001$ ).

(F) WB to assess the efficiency of each siRNA used in (D) and (E). Lysates from attached cells (out of mitotic shake off) were analyzed.

(G) The level of BubR1 at kinetochores in *Brca2*-conditional knockout MEFs. Bub1 and BubR1 levels in prometaphase kinetochores were each assessed in *Brca2*<sup>f1/f1</sup> 48 hr after infection with 100 MOI of GFP (–Cre) or Cre (+Cre)-expressing adenovirus. Scale bar, 5  $\mu$ m.

(H) Knockdown efficiency by Ad-Cre infection in (G). *Brca2* was analyzed by WB with an anti-mouse *Brca2* antibody (sh-mB2-9, Figure S1E), 48 hr after Ad-GFP (–Cre) or Ad-Cre (+Cre) infection. Intact *Brca2* is lost after Ad-Cre infection, and a faster migrating band (asterisk) is detected instead, which corresponds to the predicted size of truncated *Brca2* in the *Brca2*<sup>f1/f1</sup> allele. Lamin A/C served as a loading control. See also Figure S2.

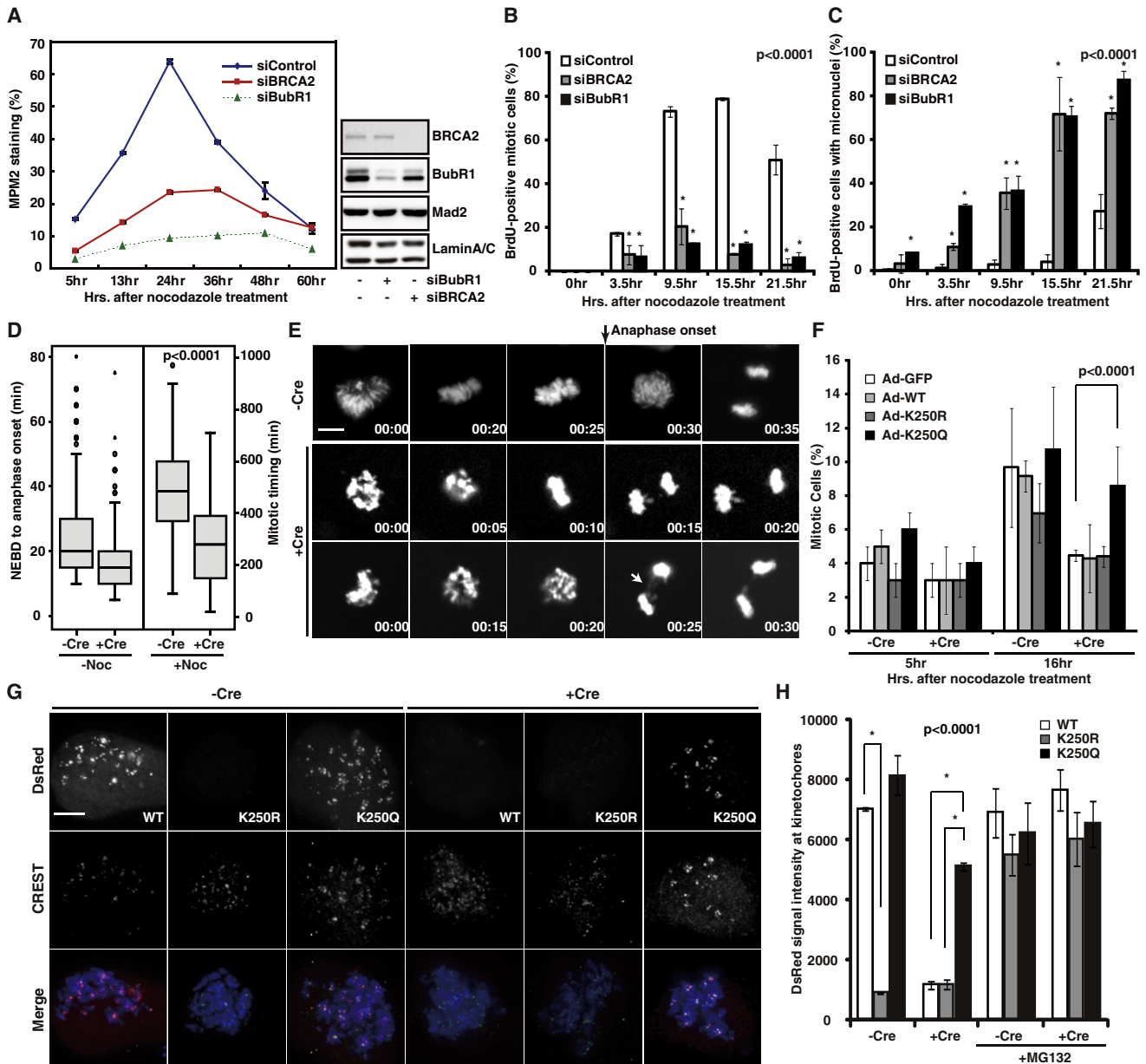


**Figure 3. BRCA2 Is Involved in the Regulation of SAC Activity**

(A) Responses to Noc by measuring the mitotic indices after Noc treatment in control, BRCA2-depleted, or BubR1-depleted HeLa cells. HeLa cells were transfected twice with siRNA for *GFP*, *BRCA2*, or *BubR1* at 24 hr intervals. Cells were then exposed to 200 ng/ml Noc, and aliquots of cells were collected at the indicated times. They were then subjected to MPM2 immunostaining and propidium iodide (PI) staining. The percentage of cells positive for MPM2 with 4C DNA is marked on the y axis, and the time after Noc treatment on the x axis. The efficiency of each siRNA was assessed (right panel).

(B) SAC activity was measured by BrdU pulse-chase and scoring of mitotic cells after Noc treatment. Thirty-six hours after transfection of indicated siRNAs in HeLa cells, they were incubated with 10  $\mu$ M BrdU for 2.5 hr, washed, and treated with Noc. Cells were fixed at the indicated time points and immunostained with anti-BrdU and anti-pH3. BrdU-positive, pH3-positive cells were scored and depicted as histograms. x axis, time after Noc treatment; y axis, percentage of BrdU-positive/pH3-positive mitotic cells. Asterisks mark the significant p values ( $p < 0.0001$ ) when compared to the cells transfected with control siRNA.

(C) Marked increase of micronuclei in BRCA2-depleted or BubR1-depleted HeLa cells. Micronuclei were detected by DAPI staining. The results are from two independent experiments (mean  $\pm$  SEM;  $n \geq 200$  BrdU-positive cells).

(D and E) MEFs from *Brca2*-conditional knockout mice were infected with *GFP*- ( $-Cre$ ) or *Cre*-expressing adenovirus ( $+Cre$ ) and subjected to live imaging in the presence or absence of Noc treatment. Recording started 36 hr postinfection and continued for 18 hr. (D) Box plot distributions of statistical mitotic timing from NEBD to anaphase onset. Without Noc treatment, mitosis required average 25 min in Ad-GFP infected MEFs ( $-Cre$ ,  $n = 242$ ) and approximately 17 min in *Brca2*-deficient MEFs ( $+Cre$ ,  $n = 168$ ) ( $-Noc$ ). When cells were exposed to Noc during recording, control MEFs ( $-Cre$ ,  $n = 74$ ) stayed in mitosis for over 500 min. *Brca2*-deficient MEFs ( $+Cre$ ,  $n = 86$ ) exited from mitosis (chromosome decondensation) within 267 min ( $+Noc$ ). Bars in the box represent median values. Outliers (open circle) and suspected outliers (asterisk) as determined by statistical analysis are marked. (E) Representative images captured at the indicated time points from (D) without Noc. Note the lagging chromosomes and anaphase bridges in Ad-*Cre*-infected MEFs. The timing of NEBD is set to 00:00. Scale bar, 5  $\mu$ m.

from *Brca2*<sup>f1/f1</sup> mice were infected with adenovirus expressing GFP (Ad-GFP) or Ad-Cre, and then were either challenged or left unchallenged with Noc and subjected to time-lapse microscopy. Elapsed time from nuclear envelope breakdown (NEBD) to anaphase onset (–Noc) or mitotic exit (+Noc) was measured. The duration of mitosis in untreated cells was approximately 8 min shorter in *Brca2*-deficient MEFs (Figure 3D, Ad-Cre, –Noc; Movies S2 and S3) than in control MEFs (Figure 3D, Ad-GFP; –Noc; Movie S1). Upon Noc treatment the difference became more profound; control MEFs (Ad-GFP) were arrested in mitosis for approximately 9 hr (Figure 3D, +Noc), whereas *Brca2*-depleted MEFs (Ad-Cre) were in mitosis for less than 5 hr (Figure 3D, +Noc). Lagging chromosomes and premature chromosome segregation without congression were frequently observed (57%, n = 96) in *Brca2*-deficient MEFs even without a Noc challenge (Figure 3E, +Cre). These are unlikely to be the secondary effects from DNA damage because no noticeable difference in the cell-cycle profile (Figure S3F),  $\gamma$ -H2AX staining (Figure S3G), or chromosome aberrations was observed (Figure S3H) at the time of analysis. Six days after Ad-Cre infection in *Brca2*<sup>f1/f1</sup> MEFs, radial-structured chromosomes resulting from impaired HR were observed. Together, these results support that BRCA2 contributes to the intactness of SAC and mitotic fidelity.

We reasoned that if BRCA2 is involved in BubR1 acetylation and SAC control, ectopic expression of an acetylation mimetic form of BubR1 should, at least in part, restore the weakened SAC of BRCA2-deficient cells. An acetylation mimetic form of BubR1 is created when K250 is substituted with glutamine (K250Q), whereas a lysine-to-arginine substitution prevents acetylation (Choi et al., 2009). Using these properties, we coinfecting *Brca2*<sup>f1/f1</sup> MEFs with *Ad-GFP-BubR1* (WT), *-K250R*, or *-K250Q*, with *Ad-GFP* or *Ad-Cre*, and then measured the response to Noc as in Figure 3B. We observed that *K250Q* expression (Ad-*K250Q*), but not *K250R* or even WT expression, recovered the ability of *Brca2*-depleted MEFs (+Cre) to arrest in mitosis in response to microtubule poisoning to a level comparable to *Brca2*-positive MEFs (–Cre; Figure 3F).

We then measured the protein levels after transfection of *Brca2*<sup>f1/f1</sup> MEFs with DsRed-tagged BubR1 constructs. Only the acetylation-mimetic BubR1-K250Q produced adequate levels of BubR1 at prometaphase kinetochores in *Brca2*-deficient MEFs, whereas *K250R* and the wild-type (WT) did not (Figures 3G and 3H). When proteolysis was blocked by MG132 addition, the fluorescence intensity of the WT and *K250R* was restored both at the kinetochore and cytosol (Figures 3H and S3I). The insufficient level of WT BubR1 in *Brca2*-deficient MEFs suggests that BRCA2-involved BubR1 acetylation is critically required for the stability of BubR1 in prometaphase.

### Spontaneous Cancer Development in Transgenic Mice with Disrupted BRCA2-BubR1 Binding

To investigate the consequence of BRCA2-BubR1 binding in vivo, we generated a transgenic mouse line that ectopically expresses the BubR1-binding region (B2-9). Our rationale was that the ectopically expressed B2-9 of *Brca2* would interfere with normal *Brca2*-BubR1 binding and decrease the mitotic BubR1 acetylation (Figure 4A).

Mouse cDNA corresponding to the B2-9 region of *Brca2* (amino acids 3,101–3,328) was engineered to be expressed in all tissues (Figure 4B). After analyzing 74 offspring from the transgene-injected mouse, we obtained only 2 germline-transmitted founders (Figure S4), suggesting that mB2-9-overexpressing embryos may not have survived to birth, and only the weak expressers were born. The transgenic mice (hereafter referred to as mB2-9 mice), which survived to birth, did not show apparent developmental defects. The expression of the B2-9 fragment in these two founders was confirmed by WB analysis in the thymus, brain, heart, and skin (Figure S4B).

At 71–90 weeks after birth, spontaneous tumor development was observed in mB2-9 mice, including abdominal sarcomas, cutaneous squamous cell carcinomas, gland adenocarcinomas, and splenomegaly (Figures 4C–4F; Table 1). The incidence of carcinomas and splenomegaly was much higher than that of sarcomas (Figure 4D; Table 1). A low incidence of lung papillary carcinomas in WT mice was observed, but this is because aged FVB/N mouse strain develops spontaneous lung cancer (Mahler et al., 1996). Overall, the tumor incidence was approximately 40% and 4-fold higher in mB2-9 mice (Figure 4E).

Further analyses of the splenomegalies in the mB2-9 mice indicated that they were lymphoma and leukemia. In paraffin-embedded sections it was observed that the spleens of mB2-9 mice were infiltrated by white blood cells, indicative of lymphoma (Figure 4F). In subsequent cytogenetic and flow cytometric analyses, we found that B220<sup>+</sup> cells, marker of B lymphocytes, increased dramatically, suggesting that B cell lymphomas had developed in the mB2-9 mice (Figure 4G). We also found spleens that were highly infiltrated by promyelocytes and/or megakaryocytes; Mac-1<sup>high</sup> and Gr-1<sup>high</sup> cells increased dramatically in mB2-9 splenomegaly (Figure 4H), indicating that either acute myelocytic leukemia (Somerville and Cleary, 2006) or chronic myelocytic leukemia (Shim et al., 2003) developed in mB2-9 mice.

Importantly, cancers from mB2-9 transgenic mice showed a high degree of genetic instability, as evaluated by comparative genomic hybridization (CGH) analysis: the genomic profile of the malignant soft cell tumor fluctuates severely at the chromosome level, indicating that the genomic complexity is markedly increased (Figure 4I).

We assessed whether ectopic expression of the BubR1-binding domain of *Brca2* indeed interfered with normal *Brca2*-BubR1

(F) *Brca2*<sup>f1/f1</sup> MEFs were coinfecting with *Ad-Cre* together with *WT*-, *K250R*-, or *K250Q-BubR1*-expressing adenovirus. Responses to Noc at indicated time points were assessed by measuring the mitotic index as in (B). Data are from two independent experiments (mean  $\pm$  SEM; n  $\geq$  2,084 cells).

(G and H) *Brca2*<sup>f1/f1</sup> MEFs transfected with DsRed-tagged *BubR1*, *-K250R*, or *-K250Q*, respectively, and the red fluorescence were measured with (–Cre) or without (+Cre) *Brca2* in the absence or presence of MG132. Immunostaining with CREST marks the kinetochore. (G) Representative images without MG132. Scale bar, 5  $\mu$ m. (H) Quantification of the results in (G). The results are from two independent experiments (mean  $\pm$  SEM; n  $\geq$  20 prometaphase cells). See also Figure S3.

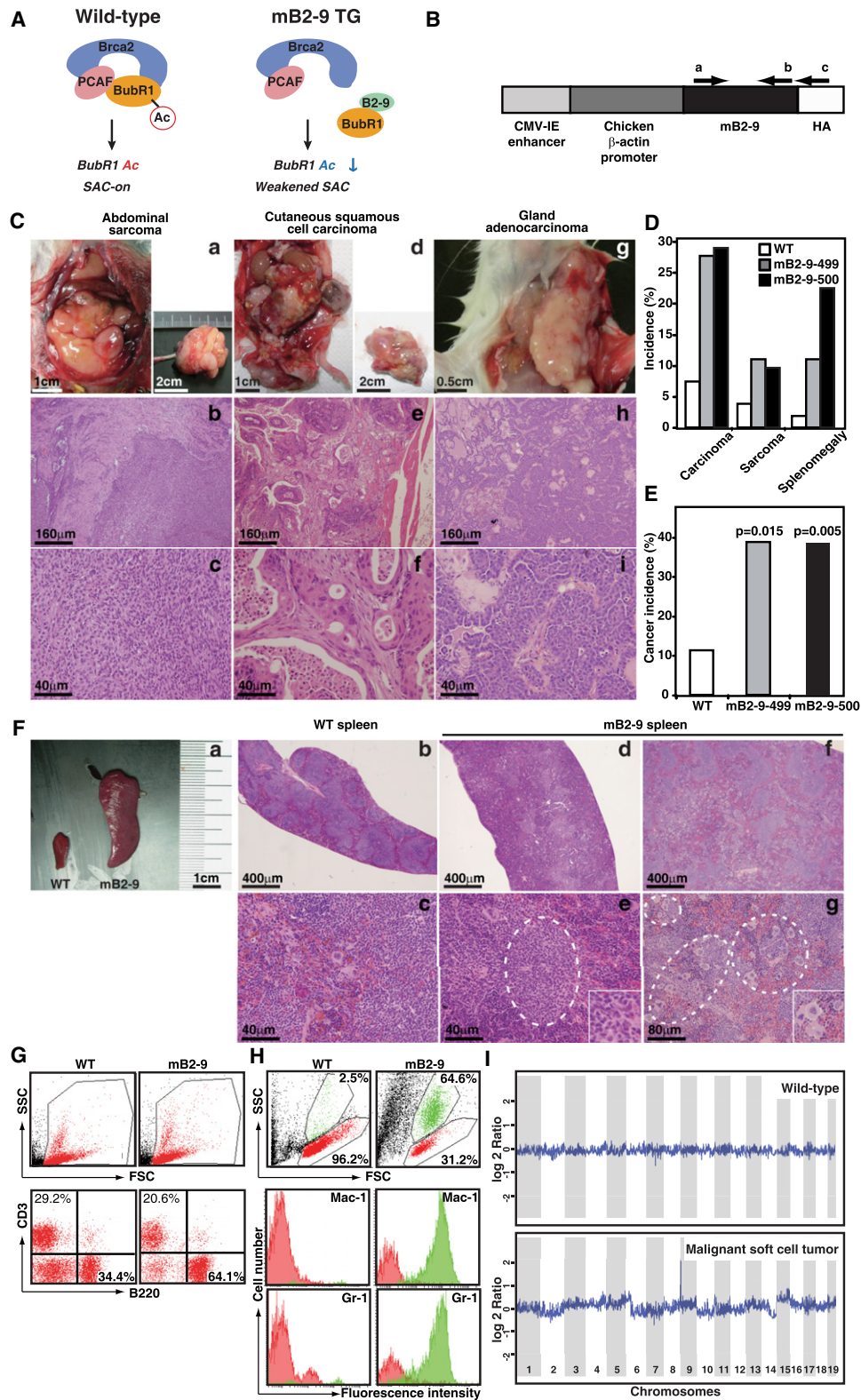


**Figure 4. Development of Spontaneous Cancers and Lymphomas/Leukemias in mB2-9 Mice**

(A) Hypothetical model predicting the status of BubR1 acetylation and SAC in mB2-9 transgenic mice.

(B) Diagram of the construct used to generate mB2-9 transgenic mice. Arrows denote PCR primer sites for genotyping (Figure S4A).

(C) Hematoxylin and eosin-stained (H&E) cancer tissue sections of mB2-9 mice. Abdominal sarcoma (a–c), cutaneous squamous cell carcinoma (d–f), and gland adenocarcinoma (g–i), are shown.

**Table 1. Spectrum of Cancers in WT and mB2-9 Mice**

	WT	mB2-9 (Line 499)	mB2-9 (Line 500)
No. of animals (%)	53 (100)	18 (100)	31 (100)
Carcinoma	4 (7.5)	5 (27.8)	9 (29.0)
Sarcoma	2 (3.8)	2 (11.1)	3 (9.7)
Splenomegaly <sup>a</sup>	1 (1.9)	2 (11.1)	7 (22.5)

<sup>a</sup> Spleens exhibited lymphocyte expansion and/or myelocyte infiltration, indicative of lymphoma/leukemia.

binding. Brca2 disappeared from BubR1 immune complexes in MEFs isolated from mB2-9 mice, whereas it was found in WT (Figure 5A). Because the N terminus of BubR1 binds to Cdc20 (Malureanu et al., 2009), binding to Cdc20 was assessed. The result showed that the binding between BubR1 and Cdc20 was not perturbed. Data from the activated splenocytes confirmed the results (Figure S5A).

We then asked whether the levels of BubR1 and BubR1 acetylation were affected in mB2-9 mice. WB analysis of MEFs revealed that the amount of BubR1 in interphase (Figure 5B, –Noc) was not noticeably different. However, the amount of BubR1 was markedly reduced in mB2-9 mice when cells were treated with Noc (Figure 5B, +Noc). The levels of Rad51, actin, and pH3 indicated that the numbers of cells analyzed were similar. Notably, mitotic BubR1 acetylation was decreased to half in mB2-9 MEFs, when compared to control (Figure 5C). Consistently, the amount of PCAF bound to BubR1 was decreased (Figure 5C,  $\alpha$ PCAF). Similar results were obtained from the activated splenocytes (Figure S5B). Altogether, these data suggest that the ectopic expression of B2-9 indeed interfered with BRCA2-BubR1 binding and BubR1 acetylation.

We next examined the timing of mitosis in transgenic MEFs. The timing from NEBD to anaphase onset was approximately 10 min shorter in mB2-9 MEFs than in WT without any treatment (Figure 5D, –Noc). When cells were challenged with Noc, mB2-9 MEFs exited from mitosis within approximately 300 min, as judged by the decondensation of chromosomes, whereas control MEFs were arrested in mitosis without dividing for more than 400 min (Figure 5D, +Noc). These results suggest that the function of BubR1 in mitotic timing and SAC activity is at least partially compromised in mB2-9 cells. Because the binding of BubR1-Cdc20 was not perturbed in mB2-9, the weakened SAC is the result of perturbed BRCA2-BubR1 binding.

Finally, we analyzed metaphase chromosome spreads from the MEFs. The result showed that mB2-9 MEFs at passage 3

already exhibit chromosome number instability: 56% of cells exhibited losses and gains of chromosomes (Figure 5E). Polyploidy was rarely observed (Figure 5E).

The C terminus of Brca2 expressed in mB2-9 mice contains the binding domain for Rad51 and a CDK1 phosphorylation site (Esashi et al., 2005, 2007) involved in regulation of HR. Because the C terminus is crucial in the stabilization of Rad51 filaments (Davies and Pellegrini, 2007; Esashi et al., 2007), we asked whether ectopic expression of B2-9 interfered with DNA repair and synergized with weakened SAC in tumorigenesis.

Cell-cycle profiles of WT and mB2-9 were similar before and after irradiation (IR), indicating that the ectopic expression of the B2-9 region did not interfere with the DNA damage response to a significant level (Figure 5F). Consistently, the level of DNA damage, assessed by  $\gamma$ -H2AX staining (Figure 5G) or the Rad51 foci formation (Figures 5H and S5C), was not significantly different from that of the control. In the metaphase chromosomes, tri-radial and quadri-radial chromosomes, the hallmarks of defective HR in Brca2 null cells (Patel et al., 1998), were not found in mB2-9 MEFs. Even after IR, we did not find radial-structured chromosomes. Only some chromatid breaks were found, and importantly, the incidence was similar to that of the WT (Figure 5I). Finally, we asked whether the actual HR activity was affected by employing DR-GFP recombination assay (Pierce et al., 1999), using transient transfection in MEFs. Flow cytometric analysis of the GFP-positive cells, representing successful HR (Figure S5D), indicated that the HR activity was not reduced in mB2-9 MEFs, compared to that of the WT (Figure 5J). Interestingly, the binding affinity of BubR1 to B2-9 was markedly higher compared to Rad51, and the mutation of serine 3291 in B2-9, the site phosphorylated by CDK1 and essential in Rad51 release before mitosis (Esashi et al., 2005), did not interfere with BubR1 binding as well (Figure S5E). These results support that B2-9 expression interfered with BRCA2-BubR1 binding more than Rad51-mediated HR.

### Clinical Relevance: Reduced BubR1 Levels in BRCA2-Mutated Breast Cancers

Our results indicate that the level of BubR1 in BRCA2-mutated cancers may be associated with the status of BRCA2. To determine whether there is any clinical relevance for our results, paraffin sections from breast cancer patient specimens (see Table S1) were analyzed for BubR1 levels by immunohistochemistry (IHC). IHC staining usually detects BubR1 in cancer cells, but not in surrounding normal tissues (Grabsch et al., 2003; Lee et al., 2009; Yamamoto et al., 2007), indicating that BubR1

(D) Incidence of cancers in mB2-9 mice. Two different founder lines were analyzed and compared with WT. Splenomegalies from mB2-9 transgenic mice were diagnosed as lymphoma/leukemia in the experiments in (F)–(H).

(E) Tumor incidence in mB2-9 mice. Data were analyzed using SPSS software. p Values represent a significant difference from WT according to Fisher's exact test.

(F) mB2-9 mice develop lymphomas and/or leukemias. Splenomegaly in mB2-9 transgenic mice (a) were analyzed. H&E of paraffin-embedded spleens (b–g). Spleens from WT mice (b and c) displayed alternating red and white pulp, mainly composed of lymphocytes (small dark-blue cells). Spleens of mB2-9 mice (d–g) were markedly enlarged, architecturally distorted, and infiltrated with atypical white blood cells (medium-sized and light-blue cells, dashed circle in e) and/or megakaryocytes (large cells, dashed circle in g). Insets in (e) and (g), magnified images of infiltrated cells.

(G) Increase of the B220-positive B cell population to 2-fold in the spleens of mB2-9 mice.

(H) Marked increase of the myelocyte cell population (high Mac-1 and high Gr-1) in the spleens of mB2-9 transgenic mice.

(I) Array CGH of WT tissue and malignant soft cell tumor from mB2-9 mouse. Plots of copy number variations, the gain/loss frequencies (y axis), relative to genomic position (x axis) were generated using CGH-Explorer software, following the methods of Chin et al. (2006). See also Figure S4.

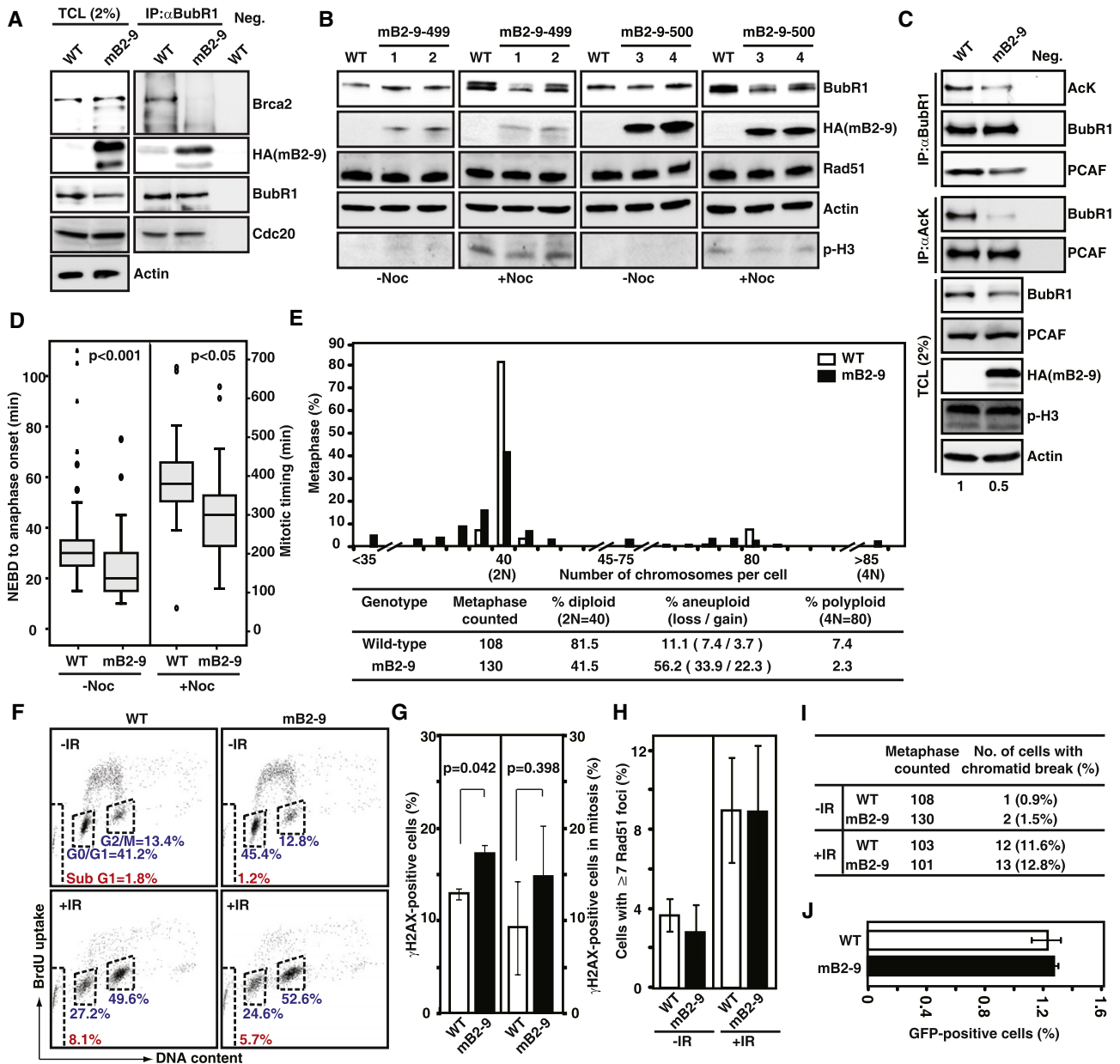


**Figure 5. mB2-9 Mice Exhibit Weak SAC Activity**

(A) MEFs isolated from WT and mB2-9 mice were subjected to IP using anti-BubR1 and WB using anti-Brca2 (sh-mB2-9), anti-HA, or anti-Cdc20. WB in TCL shows the input control (left panel).

(B) WB analysis of MEFs isolated from WT and mB2-9 siblings. Passage matched (at passage 4) WT and transgenic MEFs from two different founders were incubated for 14 hr with or without 200 ng/ml Noc and subjected to WB with the indicated antibodies.

(C) BubR1 acetylation in mitosis is markedly reduced in mB2-9 MEFs. Cells were treated with Noc, and the lysates were subjected to IP and WB as indicated. The ratio of AcK243/ total BubR1, relative to the control, is marked underneath each lane.

(D) Timing from NEBD to anaphase onset (-Noc) or mitotic exit (+Noc) was measured. Without Noc treatment the duration of mitosis was approximately 23 min in mB2-9 (n = 55) and 33 min in WT (n = 83), respectively (-Noc). When cells were exposed to Noc during recording, WT MEFs (n = 26) were arrested in mitosis for over 400 min. In comparison, mB2-9 (n = 25) exited from mitosis within 300 min (+Noc). The data are from two independent experiments.

(E) Aneuploidy in mB2-9 MEFs. The metaphase chromosome of WT (n = 108) and mB2-9 MEFs (n = 130) in passage 2 and 3 were analyzed. Chromosome numbers are depicted as histograms. Note the significant reduction of cells with normal chromosome numbers (40) in mB2-9 MEFs. The results of the histograms are summarized as a table and shown in the bottom.

(F) Cell-cycle profiles with (+IR) or without (-IR) IR (15 Gy). Cells were analyzed 18 hr post-IR.

(G) Comparison of DNA damage in WT and mB2-9 MEFs. Cells were stained with a  $\gamma$ -H2AX antibody, and  $\gamma$ -H2AX-positive cells were counted. Percentages of  $\gamma$ -H2AX-positive cells, in interphase (left) and in mitosis (right) as bar graphs. More than 2,000 cells each were scored. For scoring  $\gamma$ -H2AX-positive mitotic cells (with condensed chromosomes), 326 (WT) and 383 (mB2-9) cells were employed. Data are from two independent experiments without ectopic DNA damage (mean  $\pm$  SEM).

positivity, either mild or strong, reflects the high mitotic index of cancers. We predicted that BubR1 levels would be lower in *BRCA2*-mutated cancers than in cancers with intact *BRCA2* because BubR1 acetylation would not be maintained during proliferation. As expected, cancerous regions with high mitotic indices were positive for BubR1 IHC (Figures 6B and 6D; table in Figure 6E), whereas normal regions from the same specimens were negative (Figures 6A and 6C). The score of BubR1 immunostaining (i.e., the sum of its intensity and distribution; see also Experimental Procedures) was reduced in cancers with mutated *BRCA2* compared with those with intact *BRCA2* (Figure 6E). The *BRCA2* mutations in the analyzed samples included those that did not express the BubR1-binding domain. However, there were also mutations that did not directly affect the BubR1-binding domain (Table S1). We interpreted that the result is in agreement with the data from *Brca2*<sup>f11/f11</sup> MEFs: not only the direct BubR1-binding C terminus or the PCAF-interacting N terminus, but the entire *BRCA2*, exon 11 being essential, is required for the regulation of BubR1 acetylation. However, we do not exclude the possibility that the mutation of *BRCA2* can also affect indirect pathways leading to low score of BubR1 IHC in patients. Nevertheless, the result suggests that the score of BubR1 IHC staining could reflect the status of BubR1 acetylation and the presence of *BRCA2* mutations.

## DISCUSSION

We have shown compelling lines of evidence that *BRCA2* is required for BubR1 acetylation in mitosis and, thus, is involved in proper chromosome segregation. *BRCA2* formed a complex with BubR1 exclusively in mitosis (at prometaphase), suggesting that this tumor suppressor evolved to manifest at least two distinct functions in interphase and after chromosome condensation: it is specialized to regulate DNA repair in interphase, and after cells enter mitosis, it regulates BubR1 acetylation. In yeast, *BRCA2* is absent, and similarly, yeast Mad3 is not acetylated (Choi et al., 2009). This suggests that in metazoans, BubR1 acetylation may have evolved with the rise of *BRCA2* for the intactness of SAC and prevent from tumorigenesis.

*BRCA2*-BubR1 binding was specific to prometaphase and was found in both the kinetochore and cytosol, as is BubR1. Because BubR1 acetylation/deacetylation switches it from the inhibitor to the substrate of APC/C-Cdc20, the finding that *BRCA2*-BubR1 binding is also found in the cytosol fits with the current idea (Malureanu et al., 2009). Nevertheless, the finding that *BRCA2* is found at prometaphase kinetochores with BubR1 is important because unattached kinetochore generates diffusible “wait anaphase signal” and also may be the site to prolong SAC activation. Thus, it suggests an interesting possibility that kinetochore-bound *BRCA2* may be involved in the sustained SAC activation and signaling.

In interphase, *BRCA2* is more likely to be regulating Rad51. Therefore, it is likely that the Rad51-binding and BubR1-binding form of *BRCA2* differ, and that this is cell cycle regulated. In this vein, the requirement of the middle portion (exon 11) of *BRCA2*, which is not involved in binding to PCAF or BubR1, suggests that the phosphorylation by mitotic kinases in the middle part of *BRCA2* may be essential for *BRCA2* to function in mitosis.

In humans, mutation of *BubR1* causes a rare recessive genetic disorder named mosaic variegated aneuploidy (MVA), which manifests as growth retardation, microcephaly, childhood cancer, and constitutional mosaicism for chromosomal gains and losses (Hanks et al., 2004; Matsuura et al., 2006). Most recently, gastrointestinal cancer was reported in an adult male (Rio Frio et al., 2010), indicating that the accumulation of aneuploidy caused by SAC disruption, particularly in the case of BubR1 dysfunction, can induce tumorigenesis (Scully, 2010). However, mice with low levels of BubR1 display premature aging but do not develop spontaneous cancers on their own, although the cells are aneuploidy (Baker et al., 2004). In mB2-9 the overall level of BubR1 is intact: BubR1 level drops prematurely “in mitosis” due to decrease of BubR1 acetylation, but not in interphase. The nonacetylated BubR1 can form complex with Cdc20 as much as WT BubR1 can (Choi et al., 2009). Therefore, the existence of nonacetylated BubR1 (together with acetylated BubR1) in prometaphase weakens the SAC in mB2-9 mice. We interpreted that the reason mB2-9 mice develop spontaneous cancers while the mice with less BubR1 exhibit an aging phenotype is because nonacetylated BubR1 is able to form complexes with APC/C-Cdc20 (and MCC, the mitotic checkpoint complex) in mitosis and throughout the cell cycle, whereas hypomorphic BubR1 mice fail to achieve adequate level of APC/C-Cdc20-bound BubR1 complex formation.

Notably, the rare incidence of MVA suggests that BubR1 is essential in embryogenesis as is in mice (Baker et al., 2004; Wang et al., 2004); thus, inactivation of BubR1 as a first-hit mutation would be rarer than expected. Therefore, any factor that regulates BubR1 but is not an essential component of the SAC may be a more common target for mutation in cancers. Here, we present that *BRCA2* may be one such target. We propose that *BRCA2* in SAC regulation may be like a fine-focus knob in a microscope (Figure 6F).

Ectopic expression of the extreme C terminus of *Brca2* in mice resulted in perturbation of the normal *Brca2*-BubR1 binding. Unexpectedly, however, we observed no significant increase in DNA damage. The checkpoint response to IR was intact as well. Nonetheless, we do not exclude the possibility that DNA damage can accumulate in tumorigenesis of mB2-9 mice. Given that early-passage MEFs exhibited a significant increase in aneuploidy and malignant soft cell carcinoma displayed severe chromosome instability, it is reasonable to think

(H) Percentage of cells displaying more than seven Rad51 foci before and after IR (15 Gy). Cells were analyzed 6 hr post-IR with immunostaining with anti-Rad 51 antibody (Figure S5C). Numbers of cells analyzed are as follows: WT without IR (n = 893); mB2-9 without IR (n = 627); WT with IR (n = 1,158); mB2-9 with IR (n = 624). Data are from two independent experiments (mean ± SEM).

(I) Number of cells with chromatid breaks before and after IR (5 Gy). Values are the sum of three independent experiments.

(J) DR-GFP assay to compare HR efficiency in WT and mB2-9 MEFs. MEFs were cotransfected with 28 μg each of *DR-GFP* and *I-SceI*-expressing constructs. GFP-positive cells were analyzed by flow cytometry (see Figure S5D), and the percentage was depicted as bar graphs. The result is from three independent experiments (mean ± SEM). See also Figure S5.

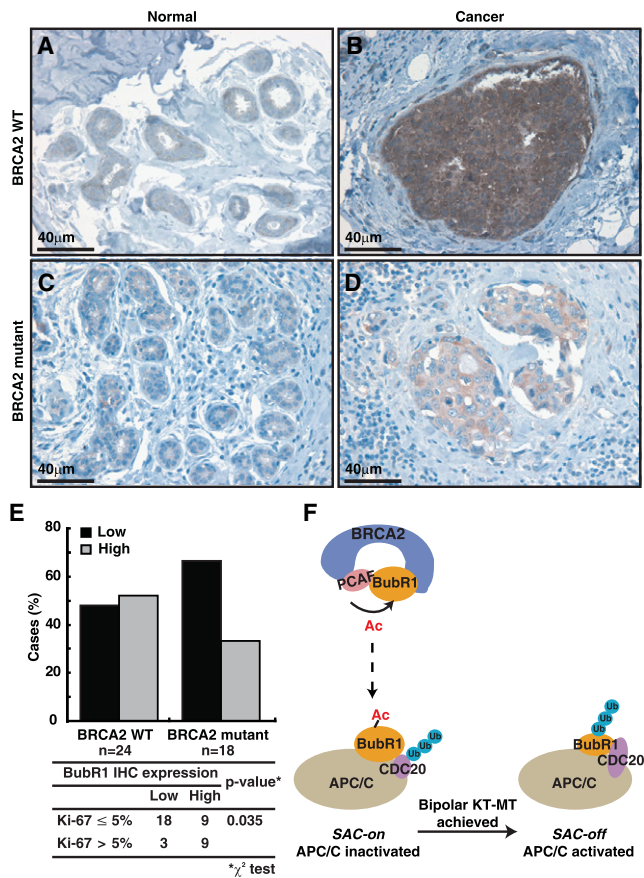


**Figure 6. BRCA2-Mutated Human Breast Cancers Display a Low Level of BubR1, Compared with Cancers with WT BRCA2**

(A–E) Breast cancer specimens were subjected to anti-BubR1 IHC and scored. Five normal tissue samples were included and compared as a control (data not shown). (A and B) Representative BubR1 IHC in cancer specimens with WT *BRCA2*. (A) Representative normal ductal epithelial region (low IHC expression,  $\times 400$ ). (B) Invasive ductal carcinoma (high IHC expression,  $\times 400$ ). (C and D) BubR1 IHC in a cancer specimen with mutant *BRCA2*. (C) Normal ductal epithelial region (low IHC expression,  $\times 400$ ). (D) Invasive ductal carcinoma (low IHC expression,  $\times 400$ ). (E) Cumulative BubR1 scores for breast cancer with mutant *BRCA2* ( $n = 18$ ) and breast cancer with WT *BRCA2* ( $n = 24$ ). Correlation between BubR1 scores and expression of Ki-67 in 39 tumor tissues is represented as a table (lower panel). (F) A model for how BRCA2 participates in mitosis. As cells enter mitosis, BRCA2 associates with BubR1 and helps the binding between PCAF and BubR1. Without intact BRCA2, BubR1 acetylation is critically impaired, and thus, the SAC activity is weakened. See also Table S1.

that the primary driving force of tumorigenesis in mB2-9 was decrease of BubR1 acetylation and weakened SAC. Thus, mB2-9 mice in a way behaved as the mouse model that dissected the mitotic role of BRCA2 from DNA repair. However, we do not rule out the possibility that the ectopically expressed B2-9 altered an unknown pathway and synergized with weakened SAC. In comparison with mB2-9, mice deficient in exon 27 exhibit defective HR, senescence, and reduced life span (Donoho et al., 2003; Morimatsu et al., 1998). Therefore, it is interpreted that the consequences of losing the C terminus and ectopically expressing it at a tolerable level (mB2-9 mice) are different.

Our analysis of human breast cancers suggests that the BRCA2-BubR1 connection might have clinical implications in the development of prognostic factors and the choice of adequate therapies. For example, IHC analysis of BubR1 may be informative for the choice of adequate treatment of breast cancers related to the status of *BRCA2*, and the development of inhibitors that specifically interfere with BubR1 deacetylation may be useful for the treatment of *BRCA2*-mutated cancers.

## EXPERIMENTAL PROCEDURES

### Statistical Analysis

SPSS software was used for statistical analyses. Student's *t* test was used unless otherwise stated. Mean  $\pm$  SEM is shown wherever required.

### Purification of Recombinant Proteins and In Vitro Acetylation Assays

For the purification of proteins from *E. coli*, BubR1 ( $\Delta$ BR2, amino acids 1–514), B2-9 (BRCA2 C terminus), BRCA2 (B2-N1, amino acids 1–500), BRCA2 (B2-N2, amino acids 290–453), and PCAF (amino acids 352–832) were subcloned into pGEX 4T-1 (Amersham) and purified as GST-fusion proteins. In addition the BubR1 deletion mutant  $\Delta$ BR1-5 was subcloned into pGEX 4T-1. The indicated combinations of recombinant proteins were incubated for 1 hr at 30°C in HAT buffer (250 mM Tris-HCl [pH 8.0], 50% glycerol, 0.5 mM EDTA, 5 mM dithiothreitol, and 1 mM unlabeled acetyl-coenzyme A). Proteins were separated by SDS-PAGE and analyzed by WB using an anti-acetyl lysine antibody.

### Cell Culture and Synchronization at Prometaphase

HeLa cells were cultured in DMEM supplemented with 10% v/v FBS. HeLa cells stably expressing FLAP-targeted BRCA2 were cultured in medium supplemented with 400  $\mu$ g/ml G418 (Lekomtsev et al., 2010).

To synchronize HeLa cells at prometaphase, cells were treated with thymidine (2 mM) for 16–20 hr, released for 6 hr, treated with 100 ng/ml Noc for 13 hr, and then collected by mitotic shake off.

To synchronize MEFs at prometaphase, cells were cultured in DMEM supplemented with 0.1% v/v FBS for 14 hr, followed by culture in DMEM supplemented with 20% v/v FBS for 7 hr. The cells were then treated with 250 ng/ml of Noc for 7 hr.

To synchronize mouse splenocytes, cells were cultured in RPMI supplemented with 10% v/v FBS in the presence of PMA (500 ng/ml), Ionomycin (500 ng/ml), and LPS (10  $\mu$ g/ml) for 36 hr. The cells were then treated with 250 ng/ml of Noc for an additional 7 hr.

### Immunofluorescence Microscopy

Immunofluorescent images (Choi et al., 2009; Choi and Lee, 2008) were acquired using a CoolSnap HQ cooled CCD camera on a DeltaVision Spectris Restoration microscope built around an Olympus IX70 stand (Applied Precision). Images were acquired as a series of 0.4- $\mu$ m-thick image sections and deconvolved using the iterative algorithm implemented in softWoRx software (Applied Precision).

### Time-Lapse Video Microscopy

MEFs were transfected with the pSV40-*mRFP-H2B* expression plasmid and grown in 35 mm Delta-T dishes (Bioprotechs), with or without 200 ng/ml Noc during the recording. Time-lapse images were obtained using DeltaVision (Applied Precision) every 5 or 10 min.

### Cell-Cycle Analysis after Depletion of BRCA2

HeLa cells were transfected twice with siRNA against control or *BRCA2* in 24 hr intervals. Forty-eight hours post-second siRNA transfection, cells were pulsed with 10  $\mu$ M BrdU for 1 hr then fixed in cold 70% ethanol. DNA was denatured with 3 N HCl and stained with FITC-anti-BrdU antibody and propidium iodide. In case of Brca2 conditional knockout MEFs, analysis was done 36–48 hr post-adenoviral infection, expressing *GFP* or *Cre*. We used FACS-Canto (Becton Dickinson) for flow cytometry, and the analysis was done with CellQuest software.

### Measuring Mitotic Index after Noc Treatment with BrdU Pulse-Chase

For BrdU labeling, cells were labeled with 10  $\mu$ M BrdU for 2.5 hr, then washed and incubated in Noc containing medium for indicated time points, and fixed with cold methanol. DNA was denatured with 3 N HCl for 10 min at room temperature. The cells were washed and subjected to double immunostaining with anti-BrdU and anti-pH3 antibodies.

### IHC and Scoring BubR1 IHC in Paraffin Sections of Tissues from Patients with Breast Cancer

Pathology samples from 42 patients and 5 samples of normal breast tissue distant from tumors were obtained as paraffin-embedded samples from the Seoul National University Hospital. The samples were collected according to the research protocol approved by the Institutional Review Board (H-1103-159-357). Of the 42 patients, 18 had hereditary breast cancer with a deleterious germline mutation of *BRCA2*, and 24 had sporadic breast cancer without a *BRCA2* mutation. *BRCA2* mutations were confirmed by gene sequencing. BubR1 scores in human cancer tissues were determined by IHC on 4  $\mu$ m tissue sections.

The percentage of positive staining distribution was recorded and scored as follows: a score of 0 (zero) for staining of <5%, 1 for 6%–30% staining, 2 for 30%–70% staining, and 3 for staining of >70%. The staining intensity was scored as follows: a score of 0 (zero) for absent tumor cell staining, 1 for weak staining (equivocal to normal epithelium), 2 for moderate staining, and 3 for strong staining. The results for intensity and distribution were summed, and total score was assigned as follows: 0–3, low expression of BubR1; 4–6, high expression of BubR1. Statistical analysis was carried out using nonparametric tests. Mann-Whitney U statistical analysis was used to compare differences in BubR1 scores between patients with a *BRCA2* mutation and those without. Cancer diagnosis and analysis were performed by pathologists from Asan Medical center (G. Gong) and Seoul National University Hospital (H. Lee).

### Animal Care

Mice were housed in a semi-conventional (virus antibody-free) facility. All mouse experiments were approved by the Institutional Animal Care and Use Committee of Seoul National University. We strictly followed the Seoul National University guidelines, policies, and regulations for the Care and Use of Laboratory Animals.

### SUPPLEMENTAL INFORMATION

Supplemental Information includes five figures, one table, Supplemental Experimental Procedures, and three movies and can be found with this article online at doi:10.1016/j.devcel.2012.01.009.

### ACKNOWLEDGMENTS

*Brca2*<sup>fl/fl</sup> mice were a gift from A. Berns (NCI, The Netherlands), and the I-SceI expression plasmid (pCBASce) and I-SceI reporter plasmids were from A.J. Pierce (University of Kentucky). We are grateful to Drs. M. Petronczki (Claire Hall Laboratories, London) and M. Kwon (Dana Farber Cancer Institute, Boston) for critical reading of the manuscript, and Dr. H-W. Lee (Yonsei University, Seoul, Korea) for help with generating mB2-9 transgenic mouse. This work was supported by the Basic Science Research Program (2008-0059996) and Grants from NRF of Korea (2009-0093927 and 2010-0026104). Flow cytometric analyses were supported by the RCFC (2005-0048590). E.C. was supported by the Priority Research Centers Program (2010-0029696).

Received: April 4, 2011

Revised: December 27, 2011

Accepted: January 17, 2012

Published online: February 13, 2012

### REFERENCES

Baker, D.J., Jeganathan, K.B., Cameron, J.D., Thompson, M., Juneja, S., Kopecka, A., Kumar, R., Jenkins, R.B., de Groen, P.C., Roche, P., and van

Deursen, J.M. (2004). BubR1 insufficiency causes early onset of aging-associated phenotypes and infertility in mice. *Nat. Genet.* 36, 744–749.

Chin, L., Garraway, L.A., and Fisher, D.E. (2006). Malignant melanoma: genetics and therapeutics in the genomic era. *Genes Dev.* 20, 2149–2182.

Choi, E., and Lee, H. (2008). Chromosome damage in mitosis induces BubR1 activation and prometaphase arrest. *FEBS Lett.* 582, 1700–1706.

Choi, E., Choe, H., Min, J., Choi, J.Y., Kim, J., and Lee, H. (2009). BubR1 acetylation at prometaphase is required for modulating APC/C activity and timing of mitosis. *EMBO J.* 28, 2077–2089.

Daniels, M.J., Wang, Y., Lee, M., and Venkitaraman, A.R. (2004). Abnormal cytokinesis in cells deficient in the breast cancer susceptibility protein *BRCA2*. *Science* 306, 876–879.

Davies, O.R., and Pellegrini, L. (2007). Interaction with the *BRCA2* C terminus protects RAD51-DNA filaments from disassembly by BRC repeats. *Nat. Struct. Mol. Biol.* 14, 475–483.

Davis, F.M., Tsao, T.Y., Fowler, S.K., and Rao, P.N. (1983). Monoclonal antibodies to mitotic cells. *Proc. Natl. Acad. Sci. USA* 80, 2926–2930.

Ditchfield, C., Johnson, V.L., Tighe, A., Ellston, R., Haworth, C., Johnson, T., Mortlock, A., Keen, N., and Taylor, S.S. (2003). Aurora B couples chromosome alignment with anaphase by targeting BubR1, Mad2, and Cenp-E to kinetochores. *J. Cell Biol.* 161, 267–280.

Donoho, G., Brenneman, M.A., Cui, T.X., Donoviel, D., Vogel, H., Goodwin, E.H., Chen, D.J., and Hasty, P. (2003). Deletion of *Brca2* exon 27 causes hypersensitivity to DNA crosslinks, chromosomal instability, and reduced life span in mice. *Genes Chromosomes Cancer* 36, 317–331.

Elowe, S., Hümmer, S., Uldschmid, A., Li, X., and Nigg, E.A. (2007). Tension-sensitive Plk1 phosphorylation on BubR1 regulates the stability of kinetochore microtubule interactions. *Genes Dev.* 21, 2205–2219.

Esashi, F., Christ, N., Gannon, J., Liu, Y., Hunt, T., Jasin, M., and West, S.C. (2005). CDK-dependent phosphorylation of *BRCA2* as a regulatory mechanism for recombinational repair. *Nature* 434, 598–604.

Esashi, F., Galkin, V.E., Yu, X., Egelman, E.H., and West, S.C. (2007). Stabilization of RAD51 nucleoprotein filaments by the C-terminal region of *BRCA2*. *Nat. Struct. Mol. Biol.* 14, 468–474.

Fuks, F., Milner, J., and Kouzarides, T. (1998). *BRCA2* associates with acetyltransferase activity when bound to P/CAF. *Oncogene* 17, 2531–2534.

Futamura, M., Arakawa, H., Matsuda, K., Katagiri, T., Saji, S., Miki, Y., and Nakamura, Y. (2000). Potential role of *BRCA2* in a mitotic checkpoint after phosphorylation by hBUBR1. *Cancer Res.* 60, 1531–1535.

Grabsch, H., Takeno, S., Parsons, W.J., Pomjanski, N., Boecking, A., Gabbert, H.E., and Mueller, W. (2003). Overexpression of the mitotic checkpoint genes BUB1, BUBR1, and BUB3 in gastric cancer—association with tumour cell proliferation. *J. Pathol.* 200, 16–22.

Hanks, S., Coleman, K., Reid, S., Plaja, A., Firth, H., Fitzpatrick, D., Kidd, A., Méhes, K., Nash, R., Robin, N., et al. (2004). Constitutional aneuploidy and cancer predisposition caused by biallelic mutations in BUB1B. *Nat. Genet.* 36, 1159–1161.

Hirsch, B., Shimamura, A., Moreau, L., Baldinger, S., Hag-alshiekh, M., Bostrom, B., Sencer, S., and D'Andrea, A.D. (2004). Association of biallelic *BRCA2/FANCD1* mutations with spontaneous chromosomal instability and solid tumors of childhood. *Blood* 103, 2554–2559.

Howlett, N.G., Taniguchi, T., Olson, S., Cox, B., Waisfisz, Q., De Die-Smulders, C., Persky, N., Grompe, M., Joenje, H., Pals, G., et al. (2002). Biallelic inactivation of *BRCA2* in Fanconi anemia. *Science* 297, 606–609.

Jeong, K., Jeong, J.Y., Lee, H.O., Choi, E., and Lee, H. (2010). Inhibition of Plk1 induces mitotic infidelity and embryonic growth defects in developing zebrafish embryos. *Dev. Biol.* 345, 34–48.

Jonkers, J., Meuwissen, R., van der Gulden, H., Peterse, H., van der Valk, M., and Berns, A. (2001). Synergistic tumor suppressor activity of *BRCA2* and p53 in a conditional mouse model for breast cancer. *Nat. Genet.* 29, 418–425.

Kulukian, A., Han, J.S., and Cleveland, D.W. (2009). Unattached kinetochores catalyze production of an anaphase inhibitor that requires a Mad2 template to prime Cdc20 for BubR1 binding. *Dev. Cell* 16, 105–117.

- Lampson, M.A., and Kapoor, T.M. (2005). The human mitotic checkpoint protein BubR1 regulates chromosome-spindle attachments. *Nat. Cell Biol.* 7, 93–98.
- Lee, H., Trainer, A.H., Friedman, L.S., Thistlethwaite, F.C., Evans, M.J., Ponder, B.A., and Venkitaraman, A.R. (1999). Mitotic checkpoint inactivation fosters transformation in cells lacking the breast cancer susceptibility gene, *Brca2*. *Mol. Cell* 4, 1–10.
- Lee, M., Daniels, M.J., Garnett, M.J., and Venkitaraman, A.R. (2011). A mitotic function for the high-mobility group protein HMG20b regulated by its interaction with the BRC repeats of the BRCA2 tumor suppressor. *Oncogene* 30, 3360–3369.
- Lee, Y.K., Choi, E., Kim, M.A., Park, P.G., Park, N.H., and Lee, H. (2009). BubR1 as a prognostic marker for recurrence-free survival rates in epithelial ovarian cancers. *Br. J. Cancer* 101, 504–510.
- Lekomtsev, S., Guizetti, J., Pozniakovsky, A., Gerlich, D.W., and Petronczki, M. (2010). Evidence that the tumor-suppressor protein BRCA2 does not regulate cytokinesis in human cells. *J. Cell Sci.* 123, 1395–1400.
- Logarinho, E., and Bousbaa, H. (2008). Kinetochore-microtubule interactions “in check” by Bub1, Bub3 and BubR1: the dual task of attaching and signaling. *Cell Cycle* 7, 1763–1768.
- Mahler, J.F., Stokes, W., Mann, P.C., Takaoka, M., and Maronpot, R.R. (1996). Spontaneous lesions in aging FVB/N mice. *Toxicol. Pathol.* 24, 710–716.
- Malureanu, L.A., Jeganathan, K.B., Hamada, M., Wasilewski, L., Davenport, J., and van Deursen, J.M. (2009). BubR1 N terminus acts as a soluble inhibitor of cyclin B degradation by APC/C(Cdc20) in interphase. *Dev. Cell* 16, 118–131.
- Matsuura, S., Matsumoto, Y., Morishima, K., Izumi, H., Matsumoto, H., Ito, E., Tsutsui, K., Kobayashi, J., Tauchi, H., Kajiwara, Y., et al. (2006). Monoallelic BUB1B mutations and defective mitotic-spindle checkpoint in seven families with premature chromatid separation (PCS) syndrome. *Am. J. Med. Genet. A.* 140, 358–367.
- Meraldi, P., Draviam, V.M., and Sorger, P.K. (2004). Timing and checkpoints in the regulation of mitotic progression. *Dev. Cell* 7, 45–60.
- Morimatsu, M., Donoho, G., and Hastay, P. (1998). Cells deleted for *Brca2* COOH terminus exhibit hypersensitivity to gamma-radiation and premature senescence. *Cancer Res.* 58, 3441–3447.
- Patel, K.J., Yu, V.P., Lee, H., Corcoran, A., Thistlethwaite, F.C., Evans, M.J., Colledge, W.H., Friedman, L.S., Ponder, B.A., and Venkitaraman, A.R. (1998). Involvement of *Brca2* in DNA repair. *Mol. Cell* 1, 347–357.
- Pellegrini, L., and Venkitaraman, A. (2004). Emerging functions of BRCA2 in DNA recombination. *Trends Biochem. Sci.* 29, 310–316.
- Peters, J.M. (2006). The anaphase promoting complex/cyclosome: a machine designed to destroy. *Nat. Rev. Mol. Cell Biol.* 7, 644–656.
- Pierce, A.J., Johnson, R.D., Thompson, L.H., and Jasin, M. (1999). XRCC3 promotes homology-directed repair of DNA damage in mammalian cells. *Genes Dev.* 13, 2633–2638.
- Rieder, C.L., and Maiato, H. (2004). Stuck in division or passing through: what happens when cells cannot satisfy the spindle assembly checkpoint. *Dev. Cell* 7, 637–651.
- Rio Frio, T., Lavoie, J., Hamel, N., Geyer, F.C., Kushner, Y.B., Novak, D.J., Wark, L., Capelli, C., Reis-Filho, J.S., Mai, S., et al. (2010). Homozygous BUB1B mutation and susceptibility to gastrointestinal neoplasia. *N. Engl. J. Med.* 363, 2628–2637.
- Rowley, M., Ohashi, A., Mondal, G., Mills, L., Yang, L., Zhang, L., Sundsbak, R., Shapiro, V., Muders, M.H., Smyrk, T., et al. (2011). Inactivation of *Brca2* promotes Trp53-associated but inhibits KrasG12D-dependent pancreatic cancer development in mice. *Gastroenterology* 140, 1303–1313.
- Scully, R. (2010). The spindle-assembly checkpoint, aneuploidy, and gastrointestinal cancer. *N. Engl. J. Med.* 363, 2665–2666.
- Shim, G.J., Wang, L., Andersson, S., Nagy, N., Kis, L.L., Zhang, Q., Mäkelä, S., Warner, M., and Gustafsson, J.A. (2003). Disruption of the estrogen receptor beta gene in mice causes myeloproliferative disease resembling chronic myeloid leukemia with lymphoid blast crisis. *Proc. Natl. Acad. Sci. USA* 100, 6694–6699.
- Somervaille, T.C., and Cleary, M.L. (2006). Identification and characterization of leukemia stem cells in murine MLL-AF9 acute myeloid leukemia. *Cancer Cell* 10, 257–268.
- Vagnarelli, P., and Earnshaw, W.C. (2004). Chromosomal passengers: the four-dimensional regulation of mitotic events. *Chromosoma* 113, 211–222.
- Venkitaraman, A.R. (2002). Cancer susceptibility and the functions of BRCA1 and BRCA2. *Cell* 108, 171–182.
- Wang, Q., Liu, T., Fang, Y., Xie, S., Huang, X., Mahmood, R., Ramaswamy, G., Sakamoto, K.M., Darzynkiewicz, Z., Xu, M., and Dai, W. (2004). BUBR1 deficiency results in abnormal megakaryopoiesis. *Blood* 103, 1278–1285.
- West, S.C. (2003). Molecular views of recombination proteins and their control. *Nat. Rev. Mol. Cell Biol.* 4, 435–445.
- Yamamoto, Y., Matsuyama, H., Chochi, Y., Okuda, M., Kawauchi, S., Inoue, R., Furuya, T., Oga, A., Naito, K., and Sasaki, K. (2007). Overexpression of BUBR1 is associated with chromosomal instability in bladder cancer. *Cancer Genet. Cytogenet.* 174, 42–47.
- Yekezare, M., and Pines, J. (2009). Escaping the firing squad: acetylation of BubR1 protects it from degradation in checkpoint cells. *EMBO J.* 28, 1991–1993.
- Yu, H. (2002). Regulation of APC-Cdc20 by the spindle checkpoint. *Curr. Opin. Cell Biol.* 14, 706–714.